

Arp 202: a TDG formed in a parent’s extended dark matter halo?

T. C. Scott¹, P. Lagos¹, S. Ramya², C. Sengupta³, S. Paudel⁴, D. K. Sahu⁵,
K. Misra⁶, J. -H. Woo⁴, and B. W. Sohn⁴

¹ *Institute of Astrophysics and Space Sciences (IA), Rua das Estrelas, 4150-762 Porto, Portugal*

² *Shanghai Astronomical Observatory, 80 Nandan Road, Shanghai 200030, China*

³ *Department of Astronomy, Yonsei University, 50 Yonsei-ro, Seodaemun-gu, Seoul, Republic of Korea*

⁴ *Korea Astronomy and Space Science Institute, 776, Daedeokdae ro, Yuseong gu, Daejeon, 305-348, Republic of Korea*

⁵ *Indian Institute of Astrophysics, Koramanagala, Bangalore 34, India*

⁶ *Aryabhata Research Institute of Observational Sciences (ARIES), Manora Peak, Nainital-263002, Uttarakhand, India*

ABSTRACT

We report on H α + [NII] imaging of the Arp 202 interacting pair and its tidal dwarf galaxy (TDG) candidate as well as a GMOS long slit spectrum from the TDG candidate, observed with the Gemini North telescope. Our H α + [NII] imaging reveals the TDG to have an elongated structure, ~ 1.9 kpc in length with the two principal star forming knots at either end. Our observations also show the TDG candidate has a recessional $V_{H\alpha} \sim 3032$ km s⁻¹, within 100 km s⁻¹ of the parent pair’s mean velocity and an oxygen abundance of $12+\log(\text{O}/\text{H}) = 8.10 \pm 0.41$. The TDG’s oxygen abundance is in good agreement with that of a star forming region in NGC 2719A, one of the parent galaxies, which has an estimated oxygen abundance of $12+\log(\text{O}/\text{H}) = 8.05 \pm 0.41$. The TDG’s $V_{H\alpha}$ and oxygen abundance confirm previous results validating the candidate as a TDG. The absence of detectable emission from the TDG in *Spitzer* 3.6 μm and 4.5 μm images together with the lack of absorption lines and weak continuum in the spectrum is consistent with absence of an old population ($\gtrsim 0.5$ Gyr). The location of the TDG within the interaction debris and the absence of indicators of an old stellar population in the TDG are consistent with a scenario in which the TDG is formed from HI stripped from the parent galaxies and within the extended dark matter halo of one of the parents as proposed by (Bournaud et al. 2003; Duc et al. 2004).

Key words: galaxies: spiral - galaxies: interactions - galaxies: kinematics and dynamics - galaxies: individual: Arp 202 H α : galaxies - spectra: galaxies galaxies: tidal dwarfs

1 INTRODUCTION

Pre-merger tidal interactions between pairs of approximately equal mass galaxies, where at least one of them is gas rich, can result in large masses of stars and gas being tidally stripping from the parent galaxies’ gas and stellar disks (e.g. Struck 1999; Hibbard et al. 2005; Duc & Mirabel 1999; Sengupta et al. 2013). Most of this tidally stripped material will eventually fall back into the potential of one or other of the pair, or at later stages the new merged galaxy. However, during this process self-gravitating bodies, with a range of masses, are observed to form within the tidal debris (e.g. Hancock et al. 2009; Smith et al. 2010a). At the top end of their mass range are bodies, with a gas content and luminous mass similar to dwarf galaxies ($\sim 10^9 M_{\odot}$) known as tidal

dwarf galaxies (TDGs) (Duc & Mirabel 1999; Duc et al. 2000; Braine et al. 2001; Duc 2012). TDG formation models propose the collapse of the HI debris into HI disk, parts of which convert to the molecular phase and further collapse to generate in-situ star formation (Bournaud et al. 2008).

TDG formation models (e.g. Dabringhausen & Kroupa 2013) also predict TDGs will contain little or no dark matter (DM), although this has proven to be difficult to confirm observationally both because their stellar and gas masses are subject to large uncertainties (Lelli et al. 2015) and it is not clear whether the assumption that these components are virialised, on which calculations of their M_{dyn} rely, is valid. Flores et al. (2016) recently pointed out many observed TDGs are probably too young for their gas and

star forming clumps to have virialised. Modelling, assuming the absence of a TDG DM halo, also shows that supernovae and stellar wind feedback, following an initial star formation (SF) burst, is insufficient to break up a TDG (Ploeckinger et al. 2014).

Because TDGs are predicted to form from chemically enriched gas originating in the parent disk(s) TDG metallicities, indicated by oxygen abundance, are expected to be approximately solar ($12+\log(\text{O}/\text{H}) = 8.69\pm 0.05$, Asplund et al. 2009) rather than the significantly sub-solar metallicities observed in normal dwarf galaxies ($12+\log(\text{O}/\text{H}) = 7.4$ to 7.9 , Lee et al. 2003). As a result metallicity is one of the principal discriminants used to distinguish TDGs from normal dwarf galaxies.

Modelling by Bournaud et al. (2003) and Duc et al. (2004) indicates that for a parent galaxy with a truncated DM halo, self gravitating bodies will form in the interaction debris and be distributed along the length of the tidal tail. However masses of these bodies will be lower than a TDG. In contrast, for a parent galaxy with an extended DM halo, a large gas mass can be carried away from the parent and accumulate at the extremity of the tidal tail. This accumulated gas at the end of tidal tail can subsequently gravitationally collapse to form a TDG. Cases where a TDG forms from pure gas debris collapse, as opposed to gas collapse in conjunction with a significant mass of stellar debris, were proposed as a separate class of TDG in Duc et al. (2004). TDG formation under the extended DM halo – pure gas collapse scenario implies both in-situ star formation and stellar population ages exclusively younger than the age of the parent interaction that gave rise to the TDG. The H I debris distribution and TDG location in Arp 105 and Arp 181 appear consistent with this scenario (Duc et al. 1997; Sengupta et al. 2013). In the case of the Arp 105 TDG a study by (Boquien et al. 2010) concluded it appeared “devoid of stellar populations older than 10^9 years”. The TDGs surrounding NGC 5291 (Duc & Mirabel 1998; Fensch et al. 2016) are likely to be examples of the pure gas collapse type, within a large scale H I debris ring formed following the collision of two galaxies.

H α and ultraviolet (UV) emission, tracing young SF on time scales of 10^7 yr and 10^8 yr respectively (Boselli et al. 2009), have been observed within evolving tidal debris, including in TDG candidates and lower mass self gravitating SF clumps (e.g. Neff et al. 2005; Hancock et al. 2009; Smith et al. 2010a). As a tracer of the most recent SF, H α is well suited, from a time scale view point, for detecting the in-situ SF predicted for TDGs. Studies of H α and UV emission can therefore assist with the validation of TDGs.

In this paper we present H α + [NII] imaging from the Himalayan Chandra Telescope¹ (HCT) of the Arp 202 interacting galaxy pair (NGC 2719 and NGC 2719A) and their TDG candidate (Figure 1), together with a Gemini Multi-Object Spectrograph (GMOS) optical spectrum for the TDG candidate. Previous UV (*GALEX*) observations revealed a very blue (FUV - g = -0.47) diffuse object at the end of a tidal tail emanating from NGC 2719A (Smith et al. 2010a), which the authors classified as a TDG candidate.

However, H α + [NII] imaging with the SARA² 0.9-m telescope at Kitt Peak (Smith et al. 2010b) and the *Spitzer* at 8 μm imaging, reported in Smith et al. (2007), failed to detect counterparts for the TDG candidate. Smith et al. (2010b) reported the TDG was at the same redshift as the Arp 202 pair with an oxygen abundance $12+\log(\text{O}/\text{H}) \sim 8.9$, which is above the $12+\log(\text{O}/\text{H})$ mean value of the Duc & Mirabel (1999) TDG sample ($12+\log(\text{O}/\text{H}) \sim 8.5$). As far as we are aware the spectrum from which the Arp 202 TDG’s redshift and metallicity was derived remains unpublished. Our GMRT H I mapping of Arp 202 (Sengupta et al. 2014) revealed an H I tidal tail, which emanates from NGC 2719A and extends to the projected position of the TDG candidate. The H I mapping provided morphological and kinematic evidence linking the interacting pair, the H I tidal tail and the H I TDG counterpart. Table 1 summaries the properties of the TDG candidate.

Schechtman-Rook & Hess (2012) presented a FUV - g vs g - r plot (their figure 11) for the UV detected TDG candidates from Smith et al. (2010a) and two other candidates, Holmberg IX and NGC 4656UV. Arp 202’s TDG candidate appears in their plot as one of the candidates with extreme blue colour, together with NGC 4656UV, Arp 305 and Holmberg IX, which is one of the strongest TDG candidates (Sabbi et al. 2008). In addition to our H I, the HCT H α + [NII] imaging and the GMOS spectrum, we utilised Sloan Digital Sky Survey (SDSS), *Spitzer* and Galaxy Evolution Explorer (*GALEX*) public archive data and images to help understand the relation between the gaseous and stellar components of the Arp 202 system.

The paper is arranged as follows: Section 2 gives details of the HCT and GMOS observations, with observational results in section 3. A discussion follows in section 4 with concluding remarks in section 5. The average of the optical radial velocities of NGC 2719 and NGC 2719A is 3097 km s^{-1} . Using this average velocity and assuming $H_0 = 75 \text{ km s}^{-1} \text{ Mpc}^{-1}$, we adopt a distance of 41.3 Mpc to NGC 2719 and NGC 2719A and the TDG. At this distance the spatial scale is $\sim 12 \text{ kpc arcmin}^{-1}$. J2000 coordinates are used throughout the paper, including in the figures.

2 OBSERVATIONS

2.1 H α + [NII] imaging and data reduction

H α + [NII] and *R* - band observations of the Arp 202 system were obtained with the 2m HCT, Hanle, India. Observations were carried out on October 9th 2015. Imaging was carried out using Himalaya Faint Object Spectrograph Camera (HFOSC), equipped with a $2K \times 4K$ SITe CCD chip, but only the central $2K \times 2K$ region (field of view of $10 \times 10 \text{ arcmin}^2$) was used for imaging. The plate scale was $0.296 \text{ arcsec pixel}^{-1}$. Multiple short exposures of Arp 202 were obtained with H α + [NII] and Bessel *R* - band filters which were then median combined to give total on target integrations of 55 min and 20 min, respectively. The H α + [NII] filter was centred at a wavelength of 6563 \AA with a bandwidth of 100 \AA . At the redshift of Arp 202 emission from the [NII] 6549.9 \AA [NII] 6585.3 \AA and H α 6564.6 \AA lines fell

¹ https://www.iiap.res.in/iao_telescope

² Southeastern Association for Research in Astronomy

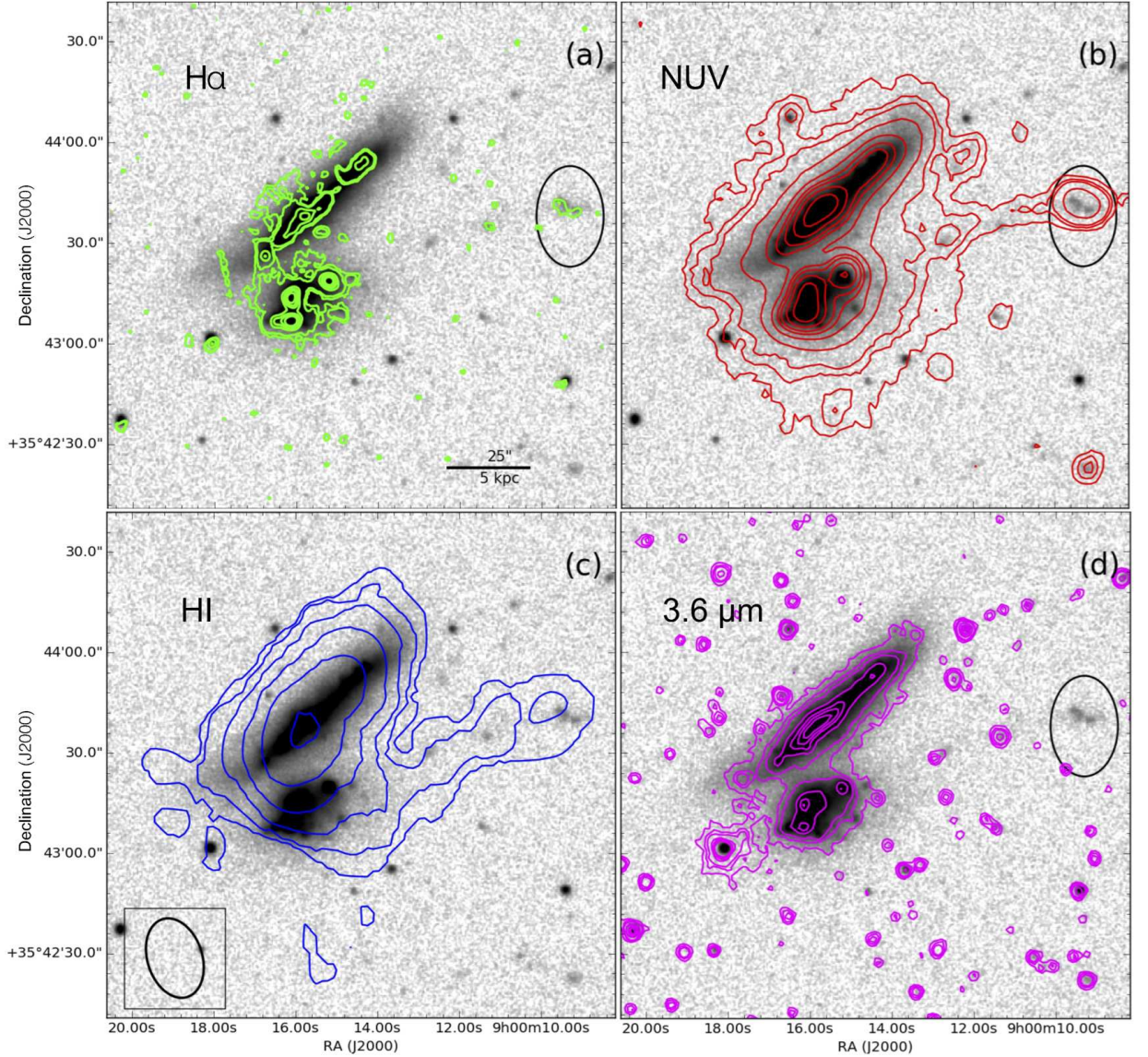


Figure 1. Arp 202: (a): $H\alpha + [NII]$ contours from a smoothed (boxcar 6×6) HCT image. The first contour is at 3σ above the background level in the smoothed image. The resolution of the contour image is ~ 1.7 arcsec. (b): Contours from an NUV (*GALEX*) image, with the first contour at 3σ above the background level. The resolution of the contour image is ~ 4 arcsec. (c): HI column density contour levels at 10^{20} atoms/cm $^2 \times (4.4, 7.5, 14.5, 26.0, 43.4, 66.6)$. The ellipse within the box indicate the size and orientation of the GMRT full width half power (FWHP) synthesised beam (23.4 arcsec \times 16.3 arcsec). (d): Contours from a *Spitzer* $3.6 \mu\text{m}$ image, with the first contour at 3σ above the background level. The resolution of the contour image is ~ 2 arcsec. In each panel the black ellipses indicate the region in which TDG candidate is projected. For all panels the background is a SDSS g - band image.

within the filter's bandwidth. The CCD calibration frames, namely, bias frames were observed throughout the night at about ~ 1 hr intervals. Morning and evening twilight flat fields were observed and used for pixel-to-pixel correction. The observations were carried out under spectroscopic conditions, although at times through passing clouds and therefore the measured $H\alpha + [NII]$ fluxes are lower limits.

The HCT data was reduced in the standard way using IRAF³ software package tasks. The reduction included bias-

subtraction, flat-field correction and alignment of the frames using IRAF tasks GEOMAP and GEOTRAN. The point spread function (PSF) of $H\alpha + [NII]$ image was matched to that of the R - band image using the IRAF GAUSS task. The sky background in individual target frames was estimated, from regions away from the galaxies and not affected by stars, which was then subtracted from the target frames. Flux calibration was carried out using the night's observations of

³ Image Reduction & Analysis Facility (IRAF) software distributed by National Optical Astronomy Observatories, which are

operated by the Association of Universities for Research in Astronomy, Inc., under co-operative agreement with the National Science Foundation

Table 1. Arp 202 TDG candidate properties

Property ^a	Units	value
$V_{radial}(HI)$	[km s ⁻¹]	3047 ± 13.6
$V_{radial}(H\alpha)$	[km s ⁻¹]	3032
RA	[h:m:s]	09:00:09.57
DEC	[d:m:s]	+35:43:42.15
Distance	[Mpc]	41.3
M_{HI}	10 ⁸ M _⊙	1.0 ± 0.5
M_* ^b	10 ⁸ M _⊙	0.4 ± 0.2
M_{dyn}	10 ⁸ M _⊙	3.9
Size(H α) major /minor	[arcsec]	4.6 × 1.3
Size(H α) major /minor	[kpc]	1.917 × 1.295
Colour	FUV - g	-0.47
Metallicity	[12 + log(O/H)]	8.10 ± 0.41
$F_{H\alpha}$	[erg cm ⁻² s ⁻¹]	2.62 ± 0.003 × 10⁻¹⁵
$L_{H\alpha}$	[erg s ⁻¹]	9.45 × 10³⁸
SFR(H α)	[10 ⁻³ M _⊙ yr ⁻¹]	7.0 ± 1

^a From this paper (bold text) otherwise from Sengupta et al. (2014)

^b Mean of M_* calculated from SDSS $g-r$, $r-i$, and $g-i$ band colours from Smith et al. (2010a) using the formulae from (Bell et al. 2003) and SDSS band solar luminosity parameters from Blanton et al. (2003).

the spectrophotometric standard star Feige 110 (Oke 1990). The H α + [NII] line image was obtained after subtracting the PSF matched and scaled version of the R - band image (which includes some line emission) from the H α + [NII] image as described by Waller (1990) and similar to the procedure adopted in Ramya et al. (2007, 2009). The flux conversion factor was estimated at 9.077×10^{-16} erg cm² s⁻¹ / (count sec⁻¹) which is similar to the value obtained in Ramya et al. (2007, 2009). As noted by James et al. (2004) scaled R - band exposures give excellent continuum subtraction for observations made during dark nights. The FWHM of the point spread function, estimated from the stars in the R band image, is ~ 5.6 pixels (1.7 arcsec).

2.2 GMOS spectrum of the TDG

A long slit spectrum for the Arp 202 TDG candidate was obtained using the Gemini Multi-Object Spectrograph (GMOS) on the 8.1 m Gemini North telescope between 25 November 2015 and 8 January 2016 (Project GN-2015B-Q-65). The on target integration time was 2.9 hr using the G5304 (B600) grating. The slit length was 330 arcsec \times 1.5 arcsec with the central wavelength set to 550.0 nm. Further details of the instrumental set up are given in Table 2. Data reduction was carried out using the Gemini software package version 1.13 within IRAF. The reduction included bias subtraction, flat-field correction, wavelength calibration and sky subtraction. Observations of Fergie 34 were used to make the flux calibration and the spectrum’s wavelength was calibrated from a CU-Ar lamp spectrum. The spectrum covers a rest frame wavelength range from ~ 4000 Å to 6900 Å with a resolution of $R_{B600} = 1688$. The slit was placed along the TDG candidate’s major axis, (PA $\sim 59.1^\circ$), inferred from NUV (*GALEX*) imaging and centred at the position of the TDG’s NUV intensity maximum, see Figure 3(d). We did not use the observation obtained on January 8th 2016, because [OIII] $\lambda 5007$ emission line fell within a gap between the GMOS detector chips precluding an accurate flux determination.

Table 2. Arp 202 TDG GMOS observation parameters

Property	Unit	value
Slit centre	RA [h:m:s]	09:00:09.300
Slit centre	DEC [d:m:s]	+35:43:38.000
Slit length	[arcsec]	330
Slit width	[arcsec]	1.5
PA	[$^\circ$]	59.1
Grating Optics	-	B600 G5304 array
Central Wavelength (rest frame)	-	550.0 nm
Filter	-	gg455
Spectral Resolution	R	1688
Spatial Binning	-	2
Spectral Binning	-	2
Pixel Size in Spatial Direction	arcsec	0.1454
Pixel Size in Spectral Direction	nm	0.093

3 OBSERVATIONAL RESULTS

3.1 H α + [NII] imaging (HCT)

The major SF zones traced by H α + [NII] emission in Figure 2(a) are not well isolated, with their extensions making it difficult to define the border of each individual zone. It is likely that the undetected H α + [NII] emission from less luminous HII clumps, in the vicinity of the detected H α + [NII] emitting regions, extend beyond their apparent boarders (Rozas et al. 1999). Hence, we group several HII zones into one star forming complex, which we refer to from here on as “SF regions”. Following Ramya et al. (2007), we selected the H α + [NII] emission from SF regions based on the criteria that the emission is centrally peaked; the boundary of the region is set where the flux falls to 2σ compared to the background (i.e. above $\sim 10^{-17}$ erg cm⁻² s⁻¹). The dashed ellipses in Figure 2(a) enclose the boundary where the H α + [NII] emission falls below the 2σ background for six star forming regions surrounding NGC 2719 and NGC 2719A, as well as a counterpart to the TDG candidate, identified by (Smith et al. 2010a), projected ~ 83 arcsec (17 kpc) NW of NGC 2719A. The total H α fluxes for the TDG and the other star forming regions are estimated from the H α + [NII] flux within the ellipses. The SF regions, numbered 1, 2 and 3, in the image are projected against or near the edge-on optical disk of NGC 2719, while knots 4, 5 and 6 are projected against or near the optical disk of NGC 2719A. An area of low density H α + [NII] emission between knots 3 and 4 may be part of a tidal bridge between the principal pair. Figure 2(a) also shows an extensive area of low surface brightness emission N of the NGC 2719 optical centre.

We detect a faint system, above the 2σ background, in the H α + [NII] image, Figures 2(b) and (c), at the position of the TDG candidate. Figure 2(b) shows the flux distribution of TDG galaxy and Figure 2(c) shows the signal-to-noise (S/N) map for the TDG with contours at 2, 2.5, 3 and 3.5 σ above the un-smoothed background. The TDG’s H α + [NII] structure detected within the ellipse in Figure 2(a) has a major axis extent of ~ 9.6 arcsec (1.92 kpc). Both Figure 2(b and c) and the green contours from a smoothed version of H α + [NII] image in Figures 3 (a, b) show an elongated structure with two principal maxima separated by ~ 5.5 arcsec (1.1 kpc). Within this structure a ridge of emission extends ~ 3 arcsec (0.6 kpc) S from the northern maxima. There is a small isolated H α + [NII] region in Figure 3(b) with a NUV counterpart to the W of the main H α + [NII]

structure, which hints at a more extended and low surface brightness $H\alpha + [\text{NII}]$ emission beyond the main detected TDG structure

Integrated $H\alpha + [\text{NII}]$ flux, $H\alpha$ luminosity, $\text{SFR}(H\alpha)$ and dimensions for each SF region and the TDG are presented in Table 3. $H\alpha$ luminosities and $\text{SFR}(H\alpha)$ s in the table are calculated after correcting the observed $H\alpha + [\text{NII}]$ fluxes for $[\text{NII}]$ contamination. For both SF region 5 and the TDG the $[\text{NII}]$ fraction of the observed $H\alpha + [\text{NII}]$ flux was 0.04, based on their respective SDSS and GMOS spectra. We also applied this same $[\text{NII}]$ fraction correction when calculating the $H\alpha$ luminosity and $\text{SFR}(H\alpha)$ for the remaining SF regions, which do not have available spectra. An extinction correction (logarithmic reddening parameter $c(H\beta) = 0.04$) was applied in calculating $L(H\alpha)$ and $\text{SFR}(H\alpha)$ for SF region 5 based on measurements from its SDSS spectrum. No extinction correction was made for the TDG because the $c(H\beta)$ derived from its GMOS spectrum, using $H\alpha/H\beta$, was 0.00 ± 0.01 . We did not make any extinction correction for the other SF regions. The table's $\text{SFR}(H\alpha)$ values are based on the formula below derived by Kennicutt (1998) for galaxies with solar abundances and an assumed Salpeter IMF with stellar masses ranging from $0.1 - 100 M_{\odot}$:

$$\text{SFR}(H\alpha) (M_{\odot} \text{ yr}^{-1}) = 7.9 \times 10^{-42} L(H\alpha) (\text{erg s}^{-1}) \quad (1)$$

The integrated flux, $F(H\alpha + [\text{NII}])$, for the TDG from the image is $1.06 \pm 0.98 \times 10^{-15} \text{ erg cm}^{-2} \text{ s}^{-1}$, corresponding to an $L(H\alpha) = 2.08 \pm 1.92 \times 10^{38} \text{ erg s}^{-1}$ and $\text{SFR}(H\alpha) = 0.002 \pm 0.002 M_{\odot} \text{ yr}^{-1}$.

For the individual SF regions in NGC 2719 $L(H\alpha)$ is in the range $\sim 21 - 93 \times 10^{38} \text{ erg s}^{-1}$ (refer Table 3). Their estimated $\text{SFR}(H\alpha)$ s are in the range $0.02 - 0.07 M_{\odot} \text{ yr}^{-1}$. Similarly, for NGC 2719A the estimated individual SF region $L(H\alpha)$ and $\text{SFR}(H\alpha)$ s are in the range $6 - 295 \times 10^{38} \text{ erg s}^{-1}$ and $0.004 - 0.23 M_{\odot} \text{ yr}^{-1}$, respectively.

3.2 TDG spectrum (GMOS)

Figure 4 shows the GMOS 1D and 2D spectra of the TDG and identifies the main emission lines detected and used in our study. Emission line profiles across the slit and integrated emission line fluxes for the TDG from the GMOS spectrum were measured by fitting Gaussian profiles with the IRAF task FITPROFS. These emission line fluxes were corrected for extinction using the observed Balmer decrement. Then, the logarithmic reddening parameter $c(H\beta)$ was calculated from the ratio of $H\alpha/H\beta$ and $H\gamma/H\beta$, where intrinsic values of 2.86 and 0.47 for case B at 10^4 K recombination were assumed (Osterbrock & Ferland 2006). Therefore, the corrected emission line fluxes were calculated as:

$$I(\lambda)/I(H\beta) = F(\lambda)/F(H\beta) \times 10^{c(H\beta)f(\lambda)} \quad (2)$$

where $I(\lambda)$ and $F(\lambda)$ are the de-reddened flux and observed flux at a given wavelength, respectively, and $f(\lambda)$ is the reddening function given by Cardelli et al. (1989). The total TDG emission line fluxes relative to $H\beta$ from the GMOS spectrum are set out in Table 4, but because $c(H\beta)$ from $H\alpha/H\beta$ is 0.00 ± 0.01 , we assume the extinction obtained from $H\gamma/H\beta$.

From the spectrum we derive $L(H\alpha) = 9.45 \times 10^{38} \text{ erg s}^{-1}$, $\text{EW}(H\alpha) = 2052 \text{ \AA}$ and $\text{EW}(H\beta) = 89 \text{ \AA}$ for the TDG. The $[\text{SII}] 6717\lambda/6731\lambda$ flux ratio for the TDG from the fluxes

in Table 4 is 2.13, assuming $T \sim 10^4 \text{ K}$ and implies $n_e \sim 100 \text{ cm}^{-3}$. We estimate the mass of the ionized gas using the equation:

$$M(HII) = \frac{L(H\alpha)m_p}{n_e \alpha_{H\alpha}^{eff} h\nu_{H\alpha}} \quad (3)$$

where m_p = the proton mass, n_e = the electron density and $\alpha_{H\alpha}$ = the effective recombination coefficient, respectively. Applying this equation we derive $M_{HII} = 2.20 \pm 0.07 \times 10^4 M_{\odot}$ and conclude that ionized gas makes an insignificant contribution to the total mass of the TDG, see Table 1.

Figure 5 shows the Arp 202 TDG GMOS spectrum profiles across the slit for: (a): $H\alpha$; (b): $c(H\beta)$; (c): $\log([\text{OIII}]/H\beta)$; (d): $\log([\text{SII}]/H\alpha)$; (e): $\log([\text{NII}]/H\alpha)$ and (f): $v(H\alpha)$. Because the $H\beta$ line is more extended than $H\gamma$, which is only resolved in a few pixels, we show the $H\alpha/H\beta$ extinction profile in Figure 5(b). The three principal knots across the slit are marked with vertical gray lines (A, B and C) on each profile.

Figure 5(b) shows the $c(H\beta)$ profile across the TDG. The reddening parameter $c(H\beta)$ was set to 0.0 for unrealistic $H\alpha/H\beta$ values < 2.86 . We inferred a range of extinction from ~ 0.0 to 0.35 in the spectrum. It is interesting to note from Figures 5(a and b) that the local $H\alpha$ emission and extinction maxima do not coincide spatially. This suggests that the current or a recent star-burst episodes are sweeping the gas and dust out of the TDG centre into the surrounding regions. This same phenomena has been also observed in some other star-forming dwarf galaxies with single and multiple SF regions (e.g. Lagos et al. 2009, 2012, 2014, 2016).

To infer the dominant ionization source in the TDG we employed the commonly used diagnostic or BPT (Baldwin et al. 1981) diagrams (Figure 6) using the following emission-line ratios: $[\text{O III}]\lambda 5007/H\beta$, $[\text{S II}]\lambda\lambda 6717, 6731/H\alpha$ and $[\text{N II}]\lambda 6584/H\alpha$. In Figures 5(c, d, e) we show those emission-line-ratio profiles. The mean value of each emission line ratio is $\log([\text{OIII}]/H\beta) = 0.30$, $\log([\text{SII}]/H\alpha) = -0.67$ and $\log([\text{NII}]/H\alpha) = -1.43$, with a standard deviations of 0.05, 0.08 and 0.09, respectively. The profiles of these emission line ratios changes from the peak of $H\alpha$ emission to the outer part of each SF knot. The $\log([\text{OIII}]/H\beta)$ ratio decreases, while $\log([\text{SII}]/H\alpha)$ and $\log([\text{NII}]/H\alpha)$ ratios increases with distance from the $H\alpha$ maxima. This figure also shows that the ionization structure of the SF knots, in the TDG, is rather regular at 1σ level for all the ionization emission line ratios. However, the maximum in the $\log([\text{NII}]/H\alpha)$ profile is more than 2σ above the mean value. All points in the BPT diagram (Figure 6) fall within the locus predicted for young stars by photo-ionization models in the BPT diagrams (Osterbrock & Ferland 2006). Therefore, we conclude photoionization from stellar sources is the dominant excitation mechanism in the TDG. The regular emission line profiles, which can be fitted with a single Gaussian component, argue against any significant fast shocks within the GMOS slit. $12+\log(\text{O}/\text{H})$ abundance, Figure 5(e), is derived by applying the relation between the line ratio of $[\text{NII}]\lambda 6584/H\alpha$ with the oxygen abundance from Denicoló et al. (2002), i.e., $12+\log(\text{O}/\text{H}) = 9.12 + 0.73 \times \text{N2}$, with $\text{N2} = \log([\text{NII}]\lambda 6584/H\alpha)$. This gives an integrated value of $12+\log(\text{O}/\text{H})$

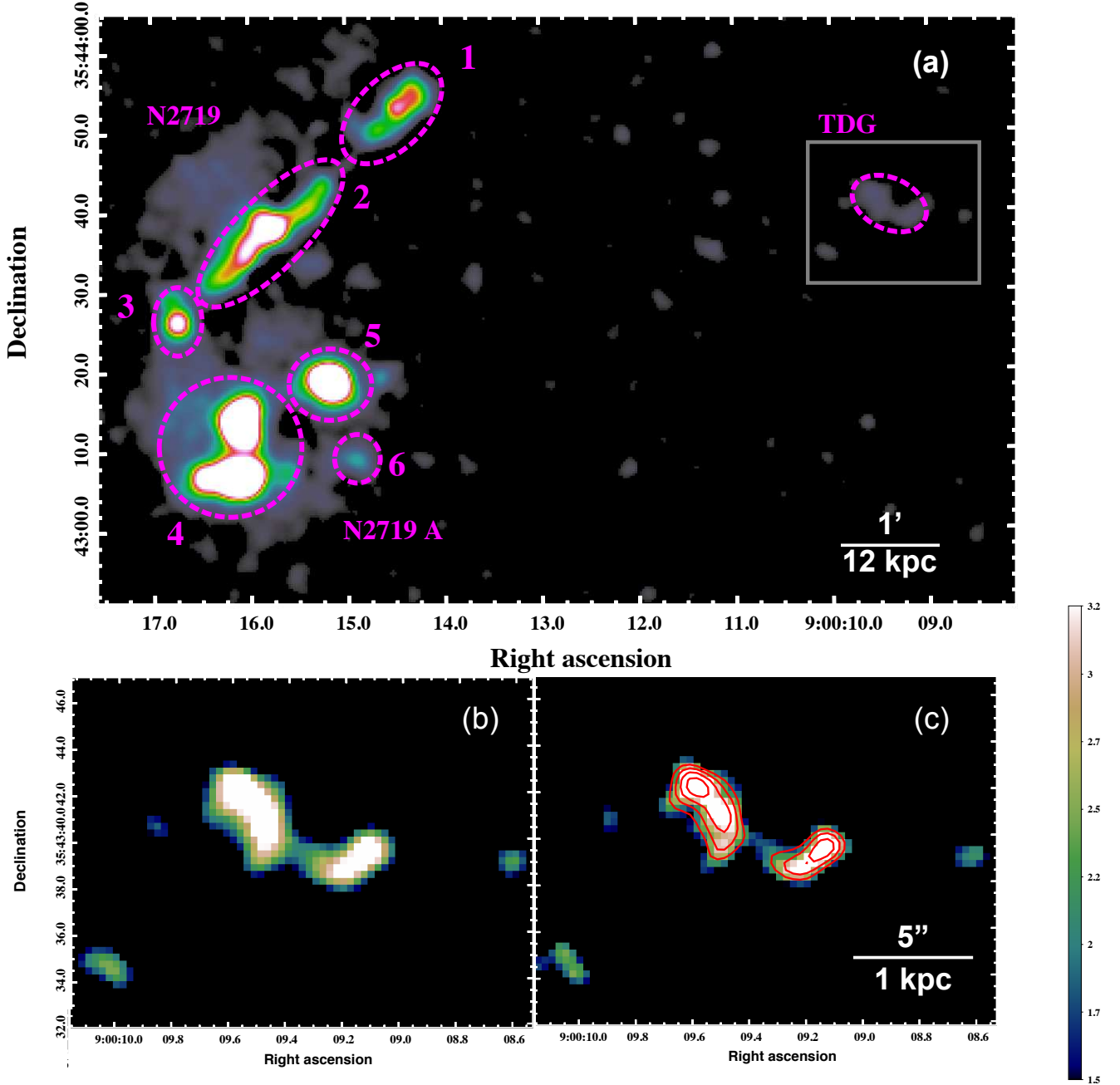


Figure 2. Continuum subtracted $H\alpha + [NII]$ images of the Arp 202 system. *Panel (a)*: identifies 6 star forming regions in the parent galaxies and the TDG, projected 83 arcsec (~ 17 kpc) to the south-west of the parent pair. Star forming knots numbered 1, 2 and 3 are associated with galaxy NGC 2719 and knots 4, 5 and 6 are associated with NGC 2719A. *Bottom left panel (b)*: shows a zoomed in to the TDG in $H\alpha + [NII]$ image. *Bottom right panel (c)*: shows the signal-to-noise map for the TDG with the contours drawn at 2, 2.5, 3.0, 3.5 σ above the background and the signal-to-noise colour scale is shown on the right.

$= 8.10 \pm 0.41$ for the TDG. Applying the same procedure to the SDSS spectrum for SF region 5 in NGC 2719A we obtain a value of $12 + \log(O/H) = 8.05 \pm 0.41$. Figure 5(f) shows the $H\alpha$ velocity, $v(H\alpha)$, profile across the slit. The TDG's mean $v(H\alpha) = 3032 \text{ km s}^{-1}$, confirming its velocity is close to those of that of the parent galaxies as reported by Smith et al. (2010a).

Using Equation 1 and the $H\alpha$ emission determined from the GMOS spectrum we estimated the total SFR for the

TDG as $SFR(H\alpha) = 0.007 \pm 0.001 M_{\odot} \text{ yr}^{-1}$, which is in reasonable agreement with the SFR($H\alpha$) derived from HCT imaging of $0.002 M_{\odot} \text{ yr}^{-1}$, see section 3.1. Ordinarily we would expect the TDG $H\alpha$ flux derived from narrow band imaging to exceed the value from a long slit spectrum because it integrates flux from a more extensive area. But as noted in section 2.1 the sky conditions for during the $H\alpha + [NII]$ imaging only allowed the lower limit for the TDGs

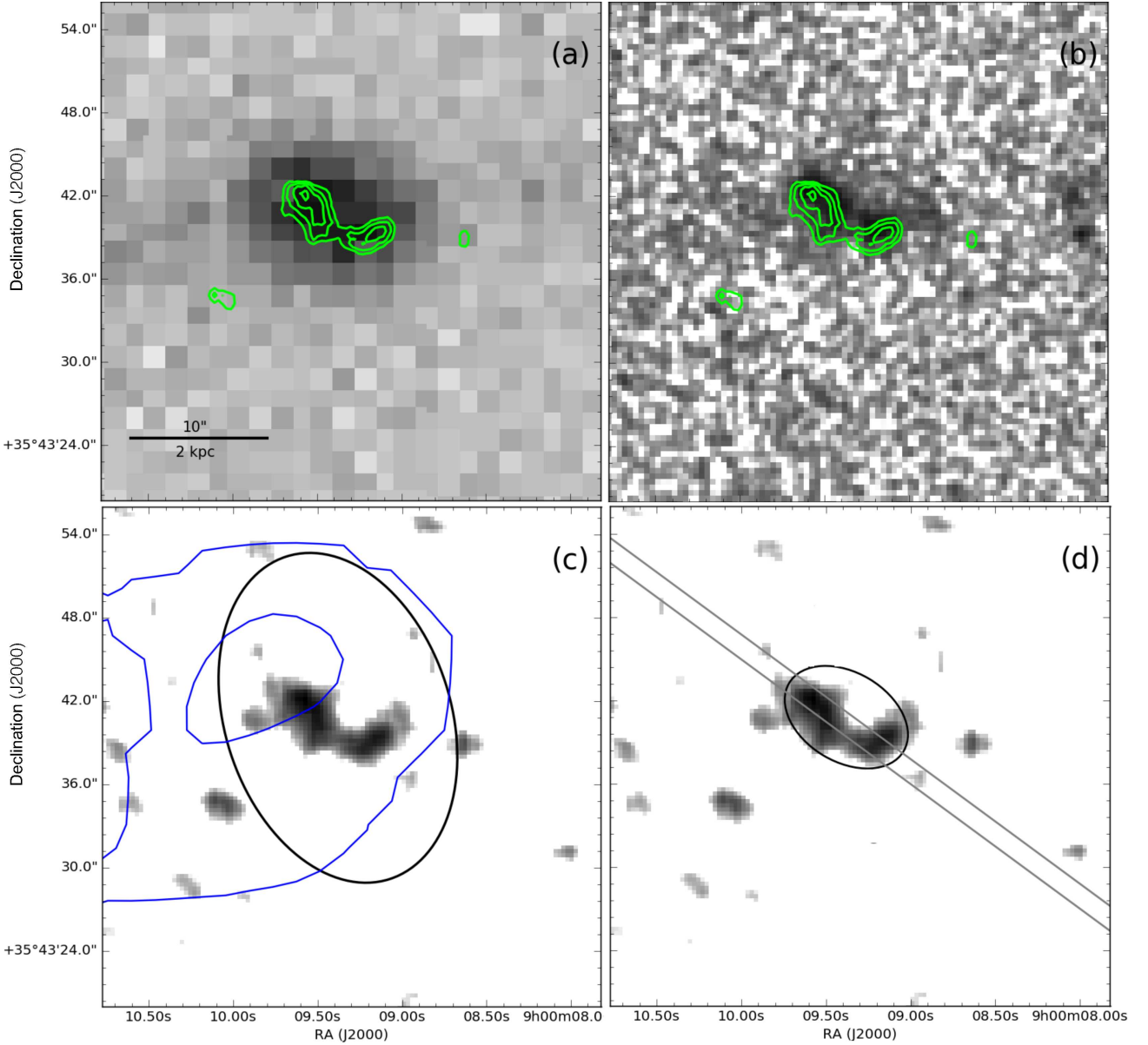


Figure 3. Arp 202 TDG: *(a)*: Contours (green) from the smoothed H α + [NII] (HCT) image on a NUV(*GALEX*) gray scale image. The contours are at 3, 4, 5 and 6 σ above the background level in the smoothed image. *(b)*: Contours (green) from smoothed H α + [NII] image on an SDSS *g* – band image. *(c)*: H I (GMRT) contours overlaid on a smoothed H α + [NII] image. Contours are at the same levels as in Figure 1, with the ellipse showing the orientation and size of the GMRT FWHP (23.4 arcsec \times 16.3 arcsec) synthesised beam. *(d)*: Smoothed H α + [NII] image. The ellipse shows the 9.6" \times 6.4" (1.9 kpc \times 1.3 kpc) region from which the H α + [NII] flux in table 3 was integrated with the parallel lines indicating GMOS slit width and orientation. The H α + [NII] images and contours are from an image smoothed with a boxcar (6 \times 6) filter.

L(H α + [NII]) and SFR(H α) to be determined from the HCT observations.

4 DISCUSSION

In the following section we discuss the relationship between the parent pair's interaction and the formation of the TDG. We were particularly interested to see whether the morphological, chemical and kinematic evidence supports the candidate being a true TDG and, if so, whether its star formation

history (SFH) is consistent with its stars being formed in-situ under the pure gas collapse scenario as the Arp 202 H I and UV morphologies suggest.

4.1 NGC 2719 and NGC 2719A

The optical radial velocity separation of the Arp 202 pair, NGC 2719 and NGC 2719A, is only 40 km s $^{-1}$. Respectively, their optical D_{25} is 1.3 arcmin (15.6 kpc) and 0.9 arcmin (11 kpc) with respective M_* values of $\sim 3.4 \times 10^9 M_{\odot}$ and $5.0 \times 10^9 M_{\odot}$ (Sengupta et al. 2014). These properties indicate

Table 3. Arp 202 SF regions: properties derived from HCT imaging.

SF region.	F(H α + [NII])		L(H α) ^a		SFR(H α) ^b	Extent ^c
	10 ⁻¹⁵ erg cm ⁻² s ⁻¹		10 ³⁸ erg s ⁻¹		M $_{\odot}$ yr ⁻¹	kpc \times kpc
TDG	1.06 \pm 0.98		2.08 \pm 1.92		0.002 \pm 0.002	1.92 \times 1.30
1	16.46 \pm 3.87		32.23 \pm 7.57		0.025 \pm 0.006	2.99 \times 1.56
2	47.97 \pm 6.60		93.95 \pm 12.92		0.074 \pm 0.010	4.83 \times 1.76
3	11.06 \pm 3.17		21.65 \pm 6.20		0.017 \pm 0.005	1.61 \times 1.04
4	150.58 \pm 11.69		294.89 \pm 22.89		0.233 \pm 0.018	3.20 \times 3.08
5	49.81 \pm 6.73		112.8 \pm 15.57		0.089 \pm 0.012	1.93 \times 1.76
6	2.86 \pm 1.61		5.61 \pm 3.16		0.004 \pm 0.002	1.31 \times 1.30

^a No extinction correction has been made, except for SF region 5 where the correction is based on $c(\text{H}\beta) = 0.04$.

^b SFR(H α) per equation 1 with $L(\text{H}\alpha) = L(\text{H}\alpha + [\text{NII}]) \times 0.96$, where 0.96 is H α fraction determined from both the TDG GMOS spectrum for the TDG and SF region 5 from its SDSS spectrum.

^c The major and minor axis of the ellipse drawn around each star forming Region.

Table 4. Arp202 TDG: integrated GMOS emission line fluxes relative to H β

Emission line (rest frame)	F(λ)/F(H β) \times 100
H γ λ 4340	49.63 \pm 4.03
H β λ 4861	100.00 \pm 4.53
[OIII] λ 4959	67.26 \pm 3.44
[OIII] λ 5007	196.71 \pm 7.04
H α λ 6563	257.42 \pm 4.44
[NII] λ 6584	10.43 \pm 0.88
[SII] λ 6717	42.46 \pm 1.71
[SII] λ 6731	19.89 \pm 1.20
F(H β) erg cm ⁻² s ⁻¹	1.77 \pm 0.03 \times 10 ⁻¹⁵
$c(\text{H}\beta)$ using H α /H β	0.00 \pm 0.01
$c(\text{H}\beta)$ using H γ /H β	0.03 \pm 0.01

both members of the pair are small lower mass galaxies with a M_{\star} ratio of $\sim 1:1.5$. The H α + [NII] bridge seen in Figure 1 between the eastern ends of the pair is also seen at lower resolution in the 3.6 μm , H I and NUV images in the same figure. This near-side tidal bridge between the galaxies and the far-side tidal tail seen in Figures 1b and 1c are typical morphologies for tidally interacting pairs (Struck 1999; Oh et al. 2008). The pair’s highly perturbed H I morphology and kinematics (Sengupta et al. 2014) indicate the parents’ most recent periape occurred well within the 0.4 Gyr to 0.7 Gyr during which H I interaction signatures are predicted to remain detectable for interactions of this magnitude (Holwerda et al. 2011). Analysis of an SDSS spectrum for a SF region within NGC 2917A also provides insights into interaction between the pair.

The SDSS spectrum for the SF region 5 in NGC 2719A is classed in SDSS as being from a galaxy star burst with an $\text{EW}(\text{H}\alpha) = 621 \pm 14 \text{ \AA}$. It is reasonable to assume this large $\text{EW}(\text{H}\alpha)$ is the result of the most recent pair interaction, with the H α emission reflecting SF on time scales of $\sim 10^7$ yr. Allowing that there may be a delay between the interaction and the onset of a SF burst as well as recognising the H I remains highly perturbed, we concluded that the most recent interaction between the pair probably occurred within a few $\times 10^8$ yr ago.

4.2 TDG Candidate

Our analysis of the TDG’s GMOS spectrum gives an oxygen abundance of $12+\log(\text{O}/\text{H}) = 8.10 \pm 0.41$, which is lower than the earlier value of 8.9 from Smith et al. (2010a). The Arp 202 parent galaxies are lower mass and gas rich galaxies, so we would expect them to have somewhat sub-solar oxygen abundances and the oxygen abundance of SF region 5 in NGC 2719A, derived from its SDSS spectrum ($12+\log(\text{O}/\text{H}) = 8.05 \pm 0.41$), is consistent with this expectation. The excellent agreement between the oxygen abundances in the TDG and SF region 5 in NGC 2719A strengthens the case for the material in the TDG having originated from the parent pair and most probably NGC 2719A. Chemical evolution modelling by Ploekinger et al. (2014) predicts no significant increase in a TDG’s integrated oxygen abundance from in-situ SF within the first 5×10^8 yrs. But, their models indicate there can be a metallicity enhancement toward the centre of the TDG as is observed in the Arp 202 TDG between knots A and B (Figure 5(e)) where the oxygen abundance reaches $12+\log(\text{O}/\text{H}) \sim 8.2$. This value is 2σ above the mean $12+\log(\text{O}/\text{H})$ abundance of ~ 8.08 ($\log(\text{NII}/\text{H}\alpha) = -1.43$; see Figure 5(e)). It is interesting that opposite trend in $12+\log(\text{O}/\text{H})$ abundance with radius is seen in a NGC 5291N TDG (Fensch et al. 2016). However, Fensch et al. (2016) note that the apparent trend is, within the errors, consistent with a homogeneous metallicity distribution.

Corroboration of the TDG’s current low SFR, referred to in section 3.2, comes from the absence of $8\mu\text{m}$ emission in the *Spitzer* image presented in Smith et al. (2007). The TDG’s SFR(FUV)⁴ ($0.011 M_{\odot} \text{ yr}^{-1}$), derived from the FUV magnitude ($m_{AB} = 20.6$) from Smith et al. (2010a), is $\sim 50\%$ higher than the SFR(H α) from GMOS. In general the derived SFR(UV) is lower than SFR(H α) in star forming regions, with the difference attributed to dust extinction of the UV emission. But for the Arp202 TDG the $c(\text{H}\beta)$ is so low that extinction cannot be a significantly contributor to the difference. Instead, the difference between SFR(FUV) and the GMOS SFR(H α) is probably due to the limited area of the TDG covered the GMOS slit and/or a rapid decline in SF within the last $\sim 10^8$ yr. A rapid decline in SF is

⁴ Based on $\text{SFR}(\text{FUV}) = 1.4 \times 10^{-28} L_{\nu}(\text{UV})$ and $f_{\nu} = 10^{-0.4(m_{AB}+46.8)}$ from (Lee et al. 2009)

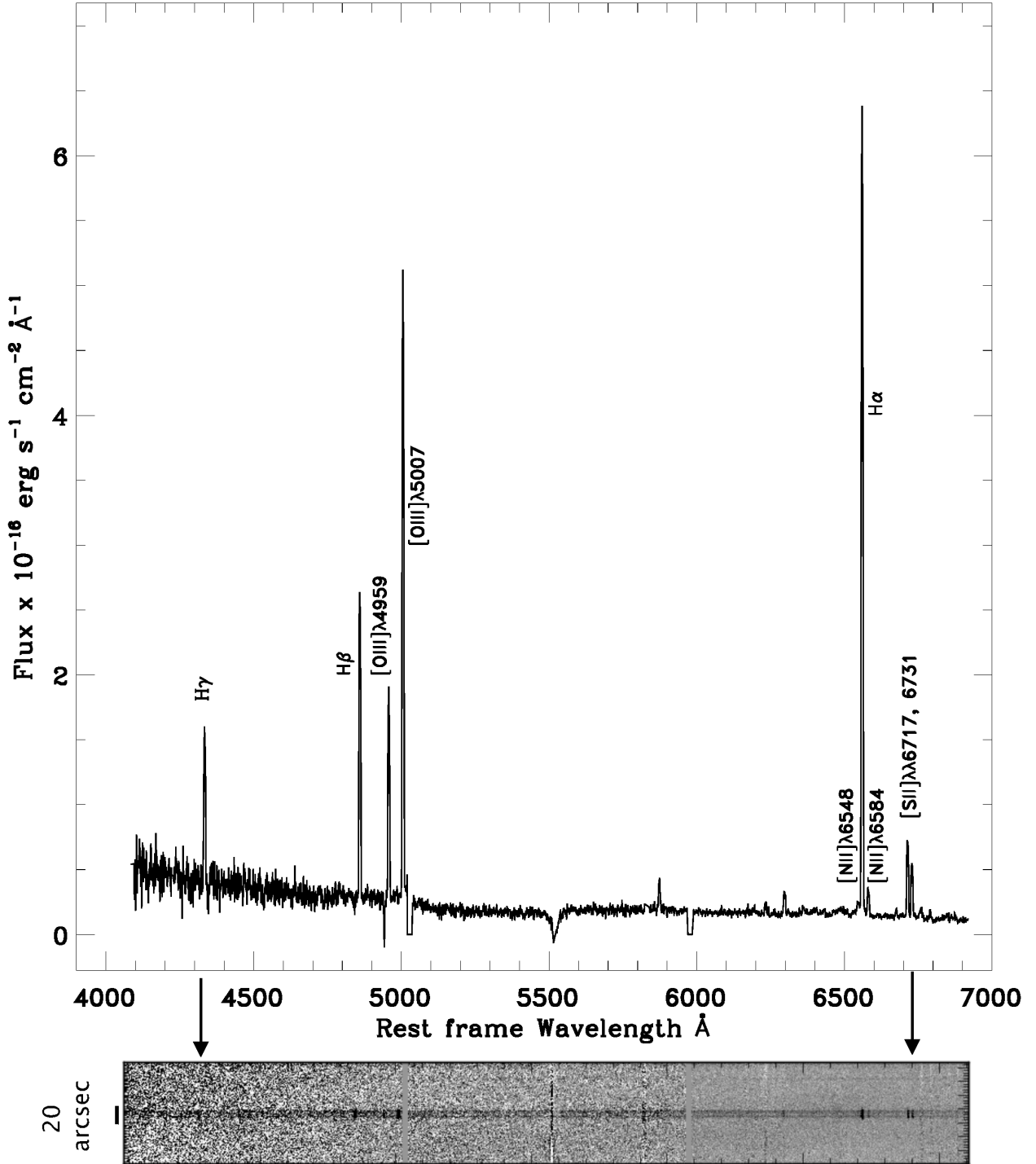


Figure 4. Arp 202 TDG GMOS spectrum: *Above*: 1D spatially integrated spectrum, with the principal emission lines labelled. *Below*: The 2D spectrum with single headed arrows identifying the H γ and [SII] doublet emission lines. Only the inner part of the slit spatial axis is shown, with the solid bar to the left of the 2D spectrum indicating the spatial extent (20 arcsec) resolved in the line profiles in Figure 5.

compatible with the idea that high SFR's in star-forming dwarfs, such as blue compact dwarf galaxies (BCDs), cannot be sustained for long periods. For example, the depletion time scales in the BCDs Mrk 36 and UM 461 (Lagos et al. 2011) are significantly less than a Hubble time ~ 0.2 Gyr and

2 Gyr, respectively. These studies suggest that these objects undergo a few or several short bursts of star formation.

Whether or not tidal debris, including TDGs, contain stellar populations older than the interaction during which they formed, provides important clues about their formation history. For example star forming regions within the

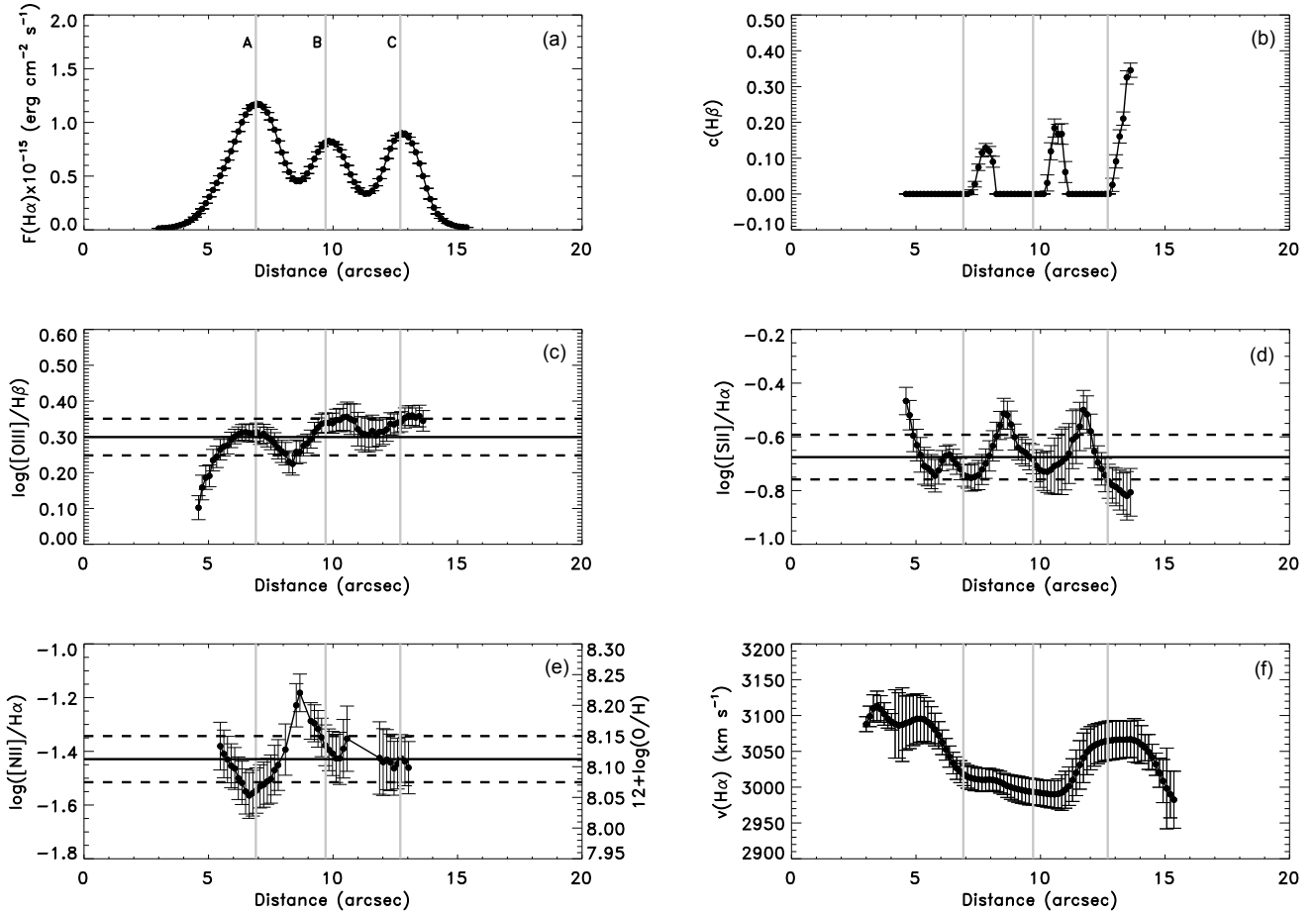


Figure 5. Arp 202 TDG GMOS spectrum profiles across the slit: (a): $H\alpha$; (b): $c(H\beta)$; (c): $\log([OIII]/H\beta)$; (d): $\log([SII]/H\alpha)$; (e): $\log([NII]/H\alpha)$, (f): $v(H\alpha)$ with the TDG’s systemic $H\alpha$ velocity = 3032 km s^{-1} . The maxima of three principal $H\alpha$ knots (A, B, C) across the slit are marked with vertical gray lines. Solid horizontal lines over plotted on the profiles indicate the mean values with the 1σ values indicated with dashed lined. The error bars are the 1σ uncertainties. $1 \text{ arcsec} \sim 200 \text{ pc}$.

tidal bridge between M81 and M82 contain both young and old ($> 1 \text{ Gyr}$) stellar populations, with the old population thought to be tidal stellar debris from the interaction (Makarova et al. 2002). *Spitzer* near infra-red (NIR) images at $3.6 \mu\text{m}$ and $4.5 \mu\text{m}$ trace emission from the old stellar population of a galaxy ($\gtrsim 1 \text{ Gyr}$), but they can be contaminated by PAH and dust emission, as well as emission from AGB and RGB stars formed in more recent SF bursts (Meidt et al. 2014). This contamination is most severe in strongly star forming regions, but given the current low Arp 202 TDG SFR, this contamination is expected to be minimal. Therefore, the absence of *Spitzer* $3.6 \mu\text{m}$ and $4.5 \mu\text{m}$ counterparts, see Figure 1(d) and Smith et al. (2007), indicates a low upper limit for the mass of the old stellar population. Integrating the flux in an circular aperture of 20 arcsec diameter from the TDG region we obtain total flux 8.2 and $14.1 \mu\text{Jy}$ with a 3σ sky-background 25.6 and $32.9 \mu\text{Jy}$ for the *Spitzer* 3.6 and 4.5 channels, respectively. This gives an upper limit of stellar mass of the TDG candidate $\approx 5 \times 10^6 M_{\odot}$ or an order of magnitude lower than the stellar mass estimates from photometry of SDSS images per Table 1. The absence of $3.6 \mu\text{m}$ and $4.5 \mu\text{m}$ NIR emission, the lack of absorption features in the GMOS spectrum and the weak continuum in the GMOS spectrum all

point to absence of any significant mass of old stars ($> 1 \text{ Gyr}$) in the TDG. In an effort to confirm the absence of an older stellar population we tried to apply spectral synthesis codes (STARLIGHT⁵ and FADO v.1⁶) to the Arp 202 TDG GMOS spectrum. The STARLIGHT fit produced results which was inconsistent with the evidence from other wavelengths. FADO, unlike most spectral synthesis codes, accounts for nebular continuum and is optimised for young star forming galaxies. While, the FADO results appeared to confirm the absence of an old stellar population (stellar ages $< 5 \times 10^8 \text{ yr}$), the quality of the continuum in the GMOS spectrum (signal to noise ~ 3) is too low to produce a credible fit. Consequently spectral synthesis modelling of the continuum from the GMOS spectrum could not be used to support a claim of an exclusively young stellar population.

The $H\alpha$ knot velocities do not appear follow a systematic trend across the slit, see Figure 5(f), suggesting the TDG as whole has not yet reached a virialised state.

⁵ <http://www.starlight.ufsc.br>.

⁶ Fitting Analysis using Differential evolution Optimization (FADO) (Gomes & Papaderos 2017).

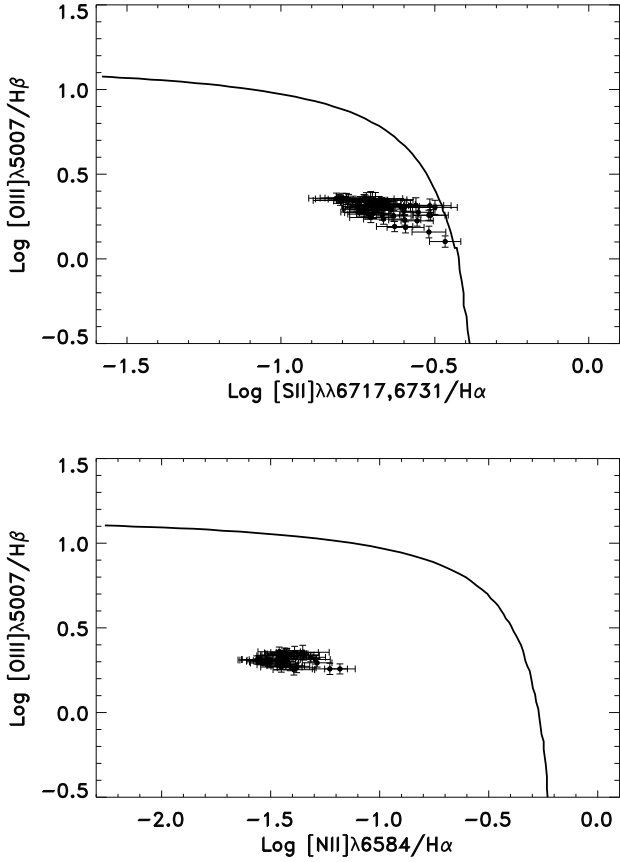


Figure 6. Arp 202 TDG BPT diagrams. *Top:* $[\text{O III}]\lambda 5007/\text{H}\beta$, $[\text{S II}]\lambda\lambda 6717,6731/\text{H}\alpha$. *Bottom:* $[\text{O III}]\lambda 5007/\text{H}\beta$, $[\text{N II}]\lambda 6584/\text{H}\alpha$. The area to the left of the solid line is the area in the diagrams predicted for young stars by photo-ionization models.

While studying the effect of H I on star formation, we find that the H I column density, $N(\text{H I})$, local maxima near the TDG position is $N(\text{H I}) \sim 7.5 \times 10^{20} \text{ atoms cm}^{-2}$, is above the threshold for SF, $N(\text{H I}) > 4 \times 10^{20} \text{ atoms cm}^{-2}$ from [Maybhate et al. \(2007\)](#). An additional finding for the Arp 202 TDG is that it has a low star formation efficiency (SFE). Based on the estimated H I masses for the parent galaxies ($7.1 \pm 0.3 \times 10^9 M_{\odot}$) ([Sengupta et al. 2014](#)) and using the sum of SFRs from Table 3 the SFE for the Arp 202 pair (SF regions 1 to 6) is $6 \times 10^{-11} \text{ yr}^{-1}$. For the TDG the estimated SFE is $7.4 \times 10^{-11} \text{ yr}^{-1}$, based on its $M(\text{H I}) = 1.0 \pm 0.5 \times 10^8 M_{\odot}$ ([Sengupta et al. 2014](#)) and $\text{SFR}(\text{H}\alpha)$ from GMOS. The TDG's SFE is unexpectedly similar to that for the interacting pair. Even accepting this, the TDG's SFE is still lower than that calculated for the Arp 305 Bridge TDG ($3 \times 10^{-10} \text{ yr}^{-1}$) from [Sengupta et al. \(2017\)](#).

The location of the Arp 202 TDG, with evidence that it is comprised of young stellar populations with a similar metallicity to a parent, at the extremity of the H I and UV tidal tail (the tail itself being essentially free of young H α + [NII] clumps) is consistent with the scenario that the TDG was formed from H I stripped from a parent and within the

parent's extended DM halo as proposed by ([Bournaud et al. 2003](#); [Duc et al. 2004](#)). This scenario predicts a TDG with stellar population consisting entirely of stars created in-situ following gravitational collapse of the H I accumulated at the tidal tail tip, i.e., the stars will be younger than the parent pair's interaction which produced the tidal tail and TDG. Evidence supporting the absence of an old stellar population in the Arp 202 TDG comes from *Spitzer* 3.6 μm and 4.5 μm non-detection, absence of absorption features in the GMOS spectrum, and weak continuum in the GMOS spectrum. An alternative to a purely gravitational collapse of the tail tip gas is that compressive tides promoted gas concentration prior to its collapse ([Renaud et al. 2009, 2015](#)). Compressive tides could be an explanation for the elongated structure of the Arp 202 TDG and the projected angular offset ($\sim 40^\circ$) between the TDG's major axis and the tidal tail. However it would require pair specific modelling to determine whether compressive tides are likely to have played a role in the TDG's formation. Based on the observational evidence to date, we conclude that a scenario in which the Arp 202 TDG formed from collapse of a large mass of gas accumulated at the tip of a tidal tail following the interaction between the parent galaxies is viable.

5 SUMMARY AND CONCLUDING REMARKS

We have imaged the Arp 202 system, including its TDG candidate, in H α + [NII] and analysed the TDG's GMOS spectrum. The GMOS observations reveal the TDG has recessional $V_{\text{H}\alpha} = 3032 \text{ km s}^{-1}$, close the parent pair's velocities and an oxygen abundance ($12 + \log(\text{O}/\text{H}) = 8.10 \pm 0.41$). The TDG's oxygen abundance is in good agreement with that from SF region 5 in NGC 2719A, one of the parent galaxies, where $12 + \log(\text{O}/\text{H}) = 8.05 \pm 0.41$. Both of these TDG properties provide positive results for key TDG validation tests and confirm the previous redshift measurement by [Smith et al. \(2010a\)](#). However the derived oxygen abundance for the TDG was lower than the $12 + \log(\text{O}/\text{H}) = 8.9$ reported in [Smith et al. \(2010a\)](#). The H α + [NII] imaging reveals the TDG to have an elongated structure $\sim 1.92 \text{ kpc}$ in length with its two principal knots at either end of the structure.

The location of the TDG at the extremity of the H I and UV tidal tail and the evidence that it lacks a significant old stellar population is consistent with the Arp 202 TDG having been formed, within the extended DM halo of one of its parent galaxies, under the pure gas collapse scenario proposed by [Bournaud et al. \(2003\)](#) and [Duc et al. \(2004\)](#). While the evidence to date does not prove this scenario, it is consistent with it. We emphasise the DM halo referred to here is that of one of the parent galaxies rather than the DM halo of the TDG itself. However, spectroscopic studies of a sample of TDGs are required to understand the extent to which the properties of TDGs formed in this way differ from cases where the TDGs contain a significant mass of old stellar tidal debris. The SFHs, chemical abundances and kinematics derived from long slit spectroscopy would assist in answering this question. However the spatial distribution of properties within TDGs is also an important aspect of the question, requiring integral field spectroscopy (IFS). Such studies have the potential to provide insights

into the impacts of initial gravitational potential and chemical abundance on the subsequent SFHs and the chemical evolution of dwarf galaxies, including TDGs.

6 ACKNOWLEDGMENTS

We are grateful to the anonymous referee for their helpful comments that have improved the paper. This work was supported by Fundação para a Ciência e a Tecnologia (FCT) through national funds (UID/FIS/04434/2013) and by FEDER through COMPETE2020 (POCI-01-0145-FEDER-007672). TS acknowledges the support by the fellowship SFRH/BPD/103385/2014 funded by FCT (Portugal) and POPH/FSE (EC). P.L. is supported by a Post-Doctoral grant SFRH/BPD/72308/2010, funded by FCT (Portugal). J.-H.W. acknowledges the support by the National Research Foundation of Korea (NRF) grant funded by the Korea government (No. 2016R1A2B3011457 and No.2017R1A5A1070354). Paudel S. acknowledges the support by Samsung Science & Technology Foundation under Project Number SSTF-BA1501-0. RS kindly acknowledges the support of NSF grant (Grant No. 11450110401) and Presidents International Fellowship Initiative (PIFI) awarded by the Chinese Academy of Sciences. We also wish to thank Jean Michel Gomes and Leanadro Cardoso for assistance with spectral synthesis codes. We thank the staff of the *HCT* and Gemini North who have made these observations possible. This research has made use of the NASA/IPAC Extragalactic Database (NED) which is operated by the Jet Propulsion Laboratory, California Institute of Technology, under contract with the National Aeronautics and Space Administration. This research has made use of the Sloan Digital Sky Survey (SDSS). Funding for the SDSS and SDSS-II has been provided by the Alfred P. Sloan Foundation, the Participating Institutions, the National Science Foundation, the U.S. Department of Energy, the National Aeronautics and Space Administration, the Japanese Monbukagakusho, the Max Planck Society, and the Higher Education Funding Council for England. The SDSS Web Site is <http://www.sdss.org/>. This research made use of APLpy, an open-source plotting package for Python hosted at <http://aplpy.github.com>

REFERENCES

- Asplund M., Grevesse N., Sauval A. J., Scott P., 2009, *ARA&A*, **47**, 481
- Baldwin J. A., Phillips M. M., Terlevich R., 1981, *PASP*, **93**, 5
- Bell E. F., McIntosh D. H., Katz N., Weinberg M. D., 2003, *ApJS*, **149**, 289
- Blanton M. R., Hogg D. W., Bahcall N. A., Brinkmann J., Britton M., Connolly A. J., Csabai I., Fukugita M., 2003, *ApJ*, **592**, 819
- Boquien M., Duc P.-A., Galliano F., Braine J., Lisenfeld U., Charmandaris V., Appleton P. N., 2010, *AJ*, **140**, 2124
- Boselli A., Boissier S., Cortese L., Buat V., Hughes T. M., Gavazzi G., 2009, *ApJ*, **706**, 1527
- Bournaud F., Duc P.-A., Masset F., 2003, *A&A*, **411**, L469
- Bournaud F., Duc P.-A., Emsellem E., 2008, *MNRAS*, **389**, L8
- Braine J., Duc P.-A., Lisenfeld U., Charmandaris V., Vallejo O., Leon S., Brinks E., 2001, *A&A*, **378**, 51
- Cardelli J. A., Clayton G. C., Mathis J. S., 1989, *ApJ*, **345**, 245
- Dabringhausen J., Kroupa P., 2013, *MNRAS*, **429**, 1858
- Denicoló G., Terlevich R., Terlevich E., 2002, *MNRAS*, **330**, 69
- Duc P.-A., 2012, *Astrophysics and Space Science Proceedings*, **28**, 305
- Duc P.-A., Mirabel I. F., 1998, *A&A*, **333**, 813
- Duc P.-A., Mirabel I. F., 1999, in Barnes J. E., Sanders D. B., eds, *IAU Symposium Vol. 186, Galaxy Interactions at Low and High Redshift*. p. 61
- Duc P.-A., Brinks E., Wink J. E., Mirabel I. F., 1997, *A&A*, **326**, 537
- Duc P.-A., Brinks E., Springel V., Pichardo B., Weilbacher P., Mirabel I. F., 2000, *AJ*, **120**, 1238
- Duc P.-A., Bournaud F., Masset F., 2004, *A&A*, **427**, 803
- Fensch J., Duc P.-A., Weilbacher P. M., Boquien M., Zackrisson E., 2016, *A&A*, **585**, A79
- Flores H., Hammer F., Fouquet S., Puech M., Kroupa P., Yang Y., Pawlowski M., 2016, *MNRAS*, **457**, L14
- Gomes J. M., Papaderos P., 2017, *A&A*, **603**, A63
- Hancock M., Smith B. J., Struck C., Giroux M. L., Hurlock S., 2009, *AJ*, **137**, 4643
- Hibbard J. E., Bianchi L., Thilker D. A., Rich R. M., Schiminovich D., Xu C. K., Neff S. G., 2005, *ApJL*, **619**, L87
- Holwerda B. W., Pirzkal N., Cox T. J., de Blok W. J. G., Weniger J., Bouchard A., Blyth S.-L., van der Heyden K. J., 2011, *MNRAS*, **416**, 2426
- James P. A., et al., 2004, *A&A*, **414**, 23
- Kennicutt Jr. R. C., 1998, *ARA&A*, **36**, 189
- Lagos P., Telles E., Muñoz-Tuñón C., Carrasco E. R., Cuisinier F., Tenorio-Tagle G., 2009, *AJ*, **137**, 5068
- Lagos P., Telles E., Nigoche-Netro A., Carrasco E. R., 2011, *AJ*, **142**, 162
- Lagos P., Telles E., Nigoche Netro A., Carrasco E. R., 2012, *MNRAS*, **427**, 740
- Lagos P., Papaderos P., Gomes J. M., Smith Castelli A. V., Vega L. R., 2014, *A&A*, **569**, A110
- Lagos P., Demarco R., Papaderos P., Telles E., Nigoche-Netro A., Humphrey A., Roche N., Gomes J. M., 2016, *MNRAS*, **456**, 1549
- Lee H., Grebel E. K., Hodge P. W., 2003, *A&A*, **401**, 141
- Lee J. C., et al., 2009, *ApJ*, **706**, 599
- Lelli F., et al., 2015, *A&A*, **584**, A113
- Makarova L. N., et al., 2002, *A&A*, **396**, 473
- Maybhate A., Masiero J., Hibbard J. E., Charlton J. C., Palma C., Knierman K. A., English J., 2007, *MNRAS*, **381**, 59
- Meidt S. E., Schinnerer E., van de Ven G., Zaritsky D., Peletier R., Knapen J. H., Sheth K., Regan M., 2014, *ApJ*, **788**, 144
- Neff S. G., Thilker D. A., Seibert M., Gil de Paz A., Bianchi L., Schiminovich D., Martin D. C., 2005, *ApJL*, **619**, L91
- Oh S. H., Kim W.-T., Lee H. M., Kim J., 2008, *ApJ*, **683**, 94
- Oke J. B., 1990, *AJ*, **99**, 1621
- Osterbrock D. E., Ferland G. J., 2006, *Astrophysics of gaseous nebulae and active galactic nuclei*
- Ploekinger S., Hensler G., Recchi S., Mitchell N., Kroupa P., 2014, *MNRAS*, **437**, 3980
- Ramya S., Sahu D. K., Prabhu T. P., 2007, *MNRAS*, **381**, 511
- Ramya S., Sahu D. K., Prabhu T. P., 2009, *MNRAS*, **396**, 97
- Renaud F., Boily C. M., Naab T., Theis C., 2009, *ApJ*, **706**, 67
- Renaud F., Bournaud F., Duc P.-A., 2015, *MNRAS*, **446**, 2038
- Rozas M., Zurita A., Heller C. H., Beckman J. E., 1999, *A&AS*, **135**, 145
- Sabbi E., Gallagher J. S., Smith L. J., de Mello D. F., Mountain M., 2008, *ApJL*, **676**, L113
- Schechtman-Rook A., Hess K. M., 2012, *ApJ*, **750**, 171
- Sengupta C., Dwarakanath K. S., Saikia D. J., Scott T. C., 2013, *MNRAS*, **431**, L1
- Sengupta C., Scott T. C., Dwarakanath K. S., Saikia D. J., Sohn B. W., 2014, *MNRAS*, **444**, 558

- Sengupta C., Scott T. C., Paudel S., Dwarakanath K. S., Saikia D. J., Sohn B. W., 2017, [MNRAS](#), **469**, 3629
- Smith B. J., Struck C., Hancock M., Appleton P. N., Charmandaris V., Reach W. T., 2007, [AJ](#), **133**, 791
- Smith B. J., Giroux M. L., Struck C., Hancock M., 2010a, [AJ](#), **139**, 1212
- Smith B. J., Giroux M. L., Struck C., Hancock M., Hurlock S., 2010b, in Smith B., Higdon J., Higdon S., Bastian N., eds, *Astronomical Society of the Pacific Conference Series Vol. 423, Galaxy Wars: Stellar Populations and Star Formation in Interacting Galaxies*. p. 257 ([arXiv:0908.3657](#))
- Struck C., 1999, [Physics Reports](#), **321**, 1
- Waller W. H., 1990, [PASP](#), **102**, 1217